Rapid Temperature Jump by Infrared Diode Laser Irradiation for Patch-Clamp Studies

Jing Yao, Beiying Liu, and Feng Qin*
Department of Physiology and Biophysical Sciences, State University of New York at Buffalo, Buffalo, New York 14214

ABSTRACT Several thermal TRP ion channels have recently been identified. These channels are directly gated by temperature, but the mechanisms have remained elusive. Studies of their temperature gating have been impeded by lack of methods for rapid alteration of temperature in live cells. As a result, only measurements of steady-state properties have been possible. To solve the problem, we have developed an optical approach that uses recently available infrared diode lasers as heat sources. By restricting laser irradiation around a single cell, our approach can produce constant temperature jumps over 50°C in submilliseconds. Experiments with several heat-gated ion channels (TRPV1–3) show its applicability for rapid temperature perturbation in both single cells and membrane patches. Compared with other laser heating approaches such as those by Raman-shifting of the Nd:YAG fundamentals, our approach has the advantage of being cost effective and applicable to live cells while providing an adequate resolution for time-resolved detection of channel activation.

INTRODUCTION

Temperature has broad effects on biological systems. Proteins such as ion channels have strong temperature dependence ($Q_{10} \approx 2$–4) (1). In addition to general thermal effects, temperature can gate specific ion channels, endowing them with the capability as thermal switches in sensory neurons for detecting ambient temperature. A number of temperature-gated ion channels have been identified, with responsiveness spanning a broad spectrum of thermal thresholds (2–10). Aside from their novel physiological functions, the discovery of these channels also raises mechanistic questions on how temperature gates a channel.

Mechanistic study of thermal sensitivity of ion channels requires controlled temperature perturbation. Conventional approaches involve resistive heating or thermal electric heating and cooling. The rate of temperature changes is generally slow, taking on the order of many seconds to minutes. As a consequence, experiments are only possible for measurements of steady-state properties. For voltage- or ligand-gated ion channels, this may be adequate because temperature plays a regulatory role. For temperature-gated ion channels, however, time-resolved measurements become important for understanding mechanisms of thermosensitivity. Much of our present knowledge on temperature gating of these channels was drawn from steady-state measurements of thermal effects on current amplitudes or other gating variables. Limited kinetic information was inferred indirectly from single-channel analysis at equilibrium (11–14). Variants of conventional thermal electric approaches have been attempted to speed up temperature changes (15), but the time responsiveness remains limited.

Fast temperature jumps are possible in aqueous solutions with laser-induced heating (16–20). The technique can be as fast as on the order of nanoseconds and has been applied to studying protein folding and unfolding dynamics in micro- to nanosecond regimes (17–20). A typical system involves Raman shifting of the Nd:YAG fundamental wavelength to generate high-power, midinfrared (1.4–1.5 μm) laser pulses. However, such a system is expensive and offers a time resolution unnecessarily high for studies of ion channel gating. Furthermore, implementation of constant temperature jumps and applicability to membrane proteins in live cells have not been shown.

We investigate here the use of infrared diode lasers as a cost-effective heat source for rapid temperature jumps. These diodes are becoming increasingly available for their application in telecommunication and come in relatively high power and a variety of wavelengths. They have been exploited for applications such as laser therapy or irradiation of peripheral nerves for pain studies (21–23). Laser-induced stimulation of nociceptive neurons in culture has also been attempted (24–27). Although these studies clearly showed possible activation of heat-sensitive currents by laser irradiation, the stimuli were insufficiently fast for resolving activation kinetics, thus preventing their use for time-resolved measurements. To circumvent the problem, we first carried out simulation to evaluate conditions for temperature jumps adequately fast for activation of temperature-gated ion channels. By using a longer wavelength (~1460 nm) than used previously (~980 nm), we showed that it is possible to achieve a submillisecond resolution for temperature jumps >60°C, giving a rate of ~55°C/ms. Both linear ramps and constant jumps were implemented. Patch-clamp studies with several heat-activated channels (TRPV1-3) were carried out to show the applicability of the system.

Submitted January 16, 2009, and accepted for publication February 11, 2009.

*Correspondence: qin@buffalo.edu

Jing Yao and Beiying Liu contributed equally to this work.

Editor: Francisco Bezanilla.

0006-3495/09/05/3611/9 $2.00

doi: 10.1016/j.bpj.2009.02.016

MATERIALS AND METHODS

Cell culture and expression

Rat vanilloid receptor type 1 (TRPV1) and type 2 (TRPV2) clones were provided by David Julius (2). Mouse TRPV3 was from Ardem Patapoutian (4). HEK293 cells were grown in Dulbecco's modified Eagle's medium (DMEM) containing 10% fetal bovine serum (Hyclone Laboratories, Logan, UT) and 1% penicillin/streptomycin, and were incubated at 37°C in a humidified incubator gassed with 5% CO_2. Transfection was made at a confluence of ~80% using the standard calcium phosphate precipitation method. Monomeric red fluorescent protein (mRFP) was cotransfected as a surface marker. Experiments took place usually 10–28 h after transfection.

The oocyte expression system was used for single-channel recording (28). *Xenopus laevis* oocytes were surgically removed, enzymatically separated using collagenase, and hand selected 1 or 2 days after harvesting for microinjection of channel cRNA. Typically, each oocyte received 10–30 ng of cRNA. The injected oocytes were incubated in ND96 solution supplemented with 2.5 mM sodium pyruvate, 100 units/mL of penicillin, and 100 μg/mL of streptomycin at 18°C for 1–2 days before use.

Electrophysiology

Conventional whole-cell and excised patch-clamp recording methods were used. Currents were amplified using an Axopatch 200B amplifier (Axon Instruments, Foster City, CA), low-pass filtered at 5 kHz through the built-in 8-pole Bessel filter, and sampled at 10–20 kHz with a multifunctional data acquisition card (National Instruments, Austin, TX). Data acquisition was controlled by custom-made software that was capable of synchronous input/output and simultaneous control of laser and patch-clamp amplifier. Pipette series resistance and capacitance were compensated using the built-in circuitry of the amplifier, and the liquid junction potential between the pipette and bath solutions was zeroed before seal formation. Pipettes were fabricated from borosilicate glass (Sutter Instruments, Novato, CA) and fire polished to a resistance between 0.5–2.5 MΩ. Currents were normally evoked from a holding potential of either −60 mV (inward) or +60 mV (outward). All voltages were defined as membrane potentials with respect to extracellular solutions.

Bath saline for whole-cell recording in HEK293 cells consisted of (mM): 150 NaCl, 5 EGTA, 10 HEPES, pH 7.4 (adjusted with NaOH). Electrodes were filled with (mM): 140 CsCl, 10 HEPES, 1 EGTA, pH 7.4 (adjusted with CsOH). The bath and pipette solutions for single-channel recording in oocytes were symmetrical and contained 100 mM NaGluconate and 10 mM NaCl instead of 150 mM NaCl, and other components were the same as the bath solution for HEK 293 cells. The pH of the HEPES-buffered solutions changed by ≤0.4 units over 22°C –55°C (7.4 at 22°C, 7.2 at 40°C, and 7 at 50°C –55°C). All chemicals were purchased from Sigma (St. Louis, MO).

Laser diode instrumentation

Fig. 1 provides a schematic drawing of the system. The laser diode was driven by a pulsed quasi-CW current power supply (Lumina Power, Bradford, MA). The controller had a rise time of 25 μs and a maximum output current of 20 A at the appliance voltage. Pulsing of the controller was controlled from a computer through the data acquisition card, which was also responsible for patch-clamp recording. The diode was mounted on a cooling block and operated at room temperature. Laser emission from the diode was collimated using an aspherical lens (f = 11.5 mm, 0.25 NA) and launched into a multimode fiber of 100 μm core diameter (0.2 NA). The other end of the fiber was cleaved and stripped to expose the fiber core. The fiber was mounted on a micromanipulator, and the tip was placed close to samples as the perfusion pipette normally was. A visible laser line (532 nm) was also coupled to the fiber to aid alignment. The beam spot on the coverslip was identified by illumination of mRFP-expressing cells using the green laser. Samples were placed at the center of the beam spot.

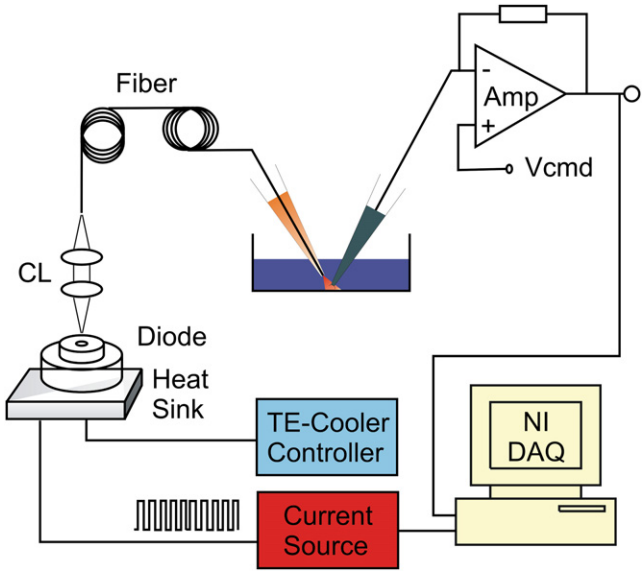

FIGURE 1 Schematic drawing of laser diode-based heating system. The diode was mounted on a temperature-controlled cooling plate. The laser beam was collimated and launched into a fiber through a pair of aspheric lenses. The fiber had a core diameter of 100 μm, and its other end was mounted onto a micromanipulator. The tip of the fiber was positioned close to the sample. The diode was powered by either a pulsed or CW current source controlled by a computer.

Constant temperature jumps were generated by irradiating the tip of an open pipette. The current through the electrode was used as a readout for feedback control. The laser was first powered on for a brief duration to reach the set temperature and was then modulated to maintain a constant pipette current. Because the pipette current depends on temperature, a constant pipette current ensures constant temperature. The sequence of the modulation pulses was stored, and subsequently used to apply temperature jumps to whole cells or membrane patches. Temperature was calibrated off line using the open pipette current and the temperature dependence of electrolyte conductivity.

In a typical experiment, a new dish of cells was placed on the microscope and the laser beam was located on the dish surface. The dish was moved around while the fluorescence of a mRFP-expressing cell was monitored. The brightest spot was marked as the center. Next, the laser control protocols for a family of constant temperature jumps were synthesized. The open pipette was positioned horizontally at the beam center and vertically at a distance typical for whole-cell recording. The position of the microscope objective was recorded for subsequent use in vertical alignment of patch electrodes. A voltage of 20–40 mV was applied to generate current through the open pipette. Finally, cells were patched, and the temperature control protocols were played back to stimulate the cell or excised patch. If necessary, an open pipette was used to verify the repeatability of temperature jumps throughout experiments.

RESULTS

Theoretical simulation

To evaluate the performance of temperature changes induced by diode laser irradiation, we numerically simulate the response using the heat conduction equation

$$c_p \frac{\partial T}{\partial t} = \kappa \nabla T + \varepsilon \times u(x, y, z),$$

where c_p is the specific heat capacity of water, κ is the thermal conductivity, ε is the optical absorption coefficient, and u is the spatial distribution of laser power. We assumed a collimated laser beam so the power could be approximated with a cylindrical geometry centered along the z axis,

$$u(x,y,z) = \begin{cases} P/\pi R^2, & \sqrt{x^2+y^2} < R \\ 0, & \text{otherwise} \end{cases},$$

where R is the fiber radius and P is the total output power. The model ignores the loss of power of laser beam due to water absorption (<3%) and temperature dependence of specific heat capacity of water.

Two types of laser diodes were considered, one with a nominal output power of 8 W at 980 nm, and the other 3 W at 1460 nm. These diodes are among the highest power commercially available and have wavelengths close to water absorption peaks. The 980 nm wavelength was similar to that used in previous studies (24,27). Fig. 2 *A* plots the simulation results for temperature rise at the beam center. With $\lambda =$ 1460 nm, the rise was almost linear and had a slope of ~280°C/ms. For a temperature jump from room temperature to 60°C (saturating temperature for temperature-gated ion channels), the irradiation duration was <150 μs. In comparison, the 980 nm laser, albeit with a higher power, resulted in a sublinear temperature increase. The absorption of water at 980 nm was <2% of that at 1460 nm (0.46/cm vs. 30/cm). The same temperature jump (22°C to 60°C) with the 980 nm laser required continuous irradiation for ~4 ms, which was ~30 times as slow as with the 1460 nm laser.

Fig. 2, *B* and *C*, shows the spatial profile of temperature distribution. With the 1460 nm diode laser, the temperature was nearly uniform within the laser beam ($\pm$50 μm). A small overshoot appeared at the edge of the beam presumably because of the assumed discontinuity of the power distribution. Outside the beam, the temperature falls sharply. The 980 nm laser produced a radial bell-shaped distribution with a gradient increasing with the maximum temperature. However, within a distance typical of cell dimensions ($\leq$10 μm), the temperature was relatively invariant (for example, at $t = 4$ ms, $T = 61.4$, 61.2, and 60.7 at $r = 0$, 5, and 10 μm, respectively). Thus, besides providing a wider spatial uniformity, the 1460 nm laser was better at producing rapid temperature jumps. The 980 nm laser at its presently available power was inadequate for detecting activation kinetics of temperature-gated ion channels ($\leq$5 ms; see below).

Experimental calibration

The launch of laser beams into fibers resulted in ~50% loss of the diode emission power due to nonoptimal coupling. We measured the actual laser-induced temperature changes by monitoring currents flowing through an open patch pipette (27,29). The beam from the diode was coupled to a 100 μm-diameter multimode fiber and the other end of the fiber was placed where the perfusion pipette was normally located. The location of the beam spot on the coverslip was identified by illumination of mRFP-expressing cells using a visible laser line (532 nm) that was launched into the same fiber. The tip of the open electrode was positioned at the beam center and at a vertical distance from the coverslip typical for whole-cell recording.

Fig. 3, *A* and *B*, shows recordings of currents from an open electrode for several laser output powers (normalized to currents at room temperature). After the laser was switched on, the current increased sharply (*black traces*). The temperature is shown in the same plot (*red/grey traces*). To calibrate the temperature from the current, we premeasured the temperature dependence of electrode current (Fig. 3 *C*). The resulting Arrhenius plot was linear, conforming to a constant activation energy for the solution. From the slope of the plot, the activation energy was estimated $E_a = 3.84$ kcal/mol ($n = 20$), equivalent to $Q_{10} = 1.23$ at $T = 25$°C. Given this estimate of E_a, the temperature was calibrated from the pipette current by

$$T = \frac{1}{\frac{1}{T_0} - \frac{R}{E_a}\log\left(\frac{I}{I_0}\right)},$$

where R is the gas constant, T_0 is the starting (room) temperature and I_0 is the pipette current at T_0. For the 1460 nm laser, the temperature rise was linear at high powers, and reached >60°C in <1 ms, corresponding to a rate of ~55°C/ms. The 980 nm laser was considerably slower and exhibited a sublinear increase (Fig. 3 *A*). The time course of the temperature changes was generally in agreement with the predictions from simulation, though the absolute rate of changes was slower due to lower output powers.

The variation of temperature within the illumination area is shown in Fig. 3 *D*. As expected, the temperature fell off radially and faster at high temperatures. For the 1460 nm laser beam, the variation was <5% within a radius $\leq$10 μm. Thus, a relatively uniform temperature jump was possible in a single cell. Because of its superior performance on both temporal resolution and spatial distribution, we used the 1460 nm laser diode for most of our subsequent experiments.

Constant temperature jumps

Without feedback control, continuous laser irradiation at a constant power results in linearly increasing temperature ramps, but electrophysiological applications often require temperature steps for simpler analysis. To achieve a constant temperature jump, we created the response with an open pipette, and the resulting laser control protocol was then played back for actual patches. Fig. 4 *A* shows a schematic of the design. The electrode current was used as a feedback signal to modulate laser power. The laser was first turned on for a brief duration until a target temperature was reached, and then the laser was pulsed on and off (pulse width modulation) to maintain the electrode current. Because the current is a sensitive function of temperature, the rapid modulation

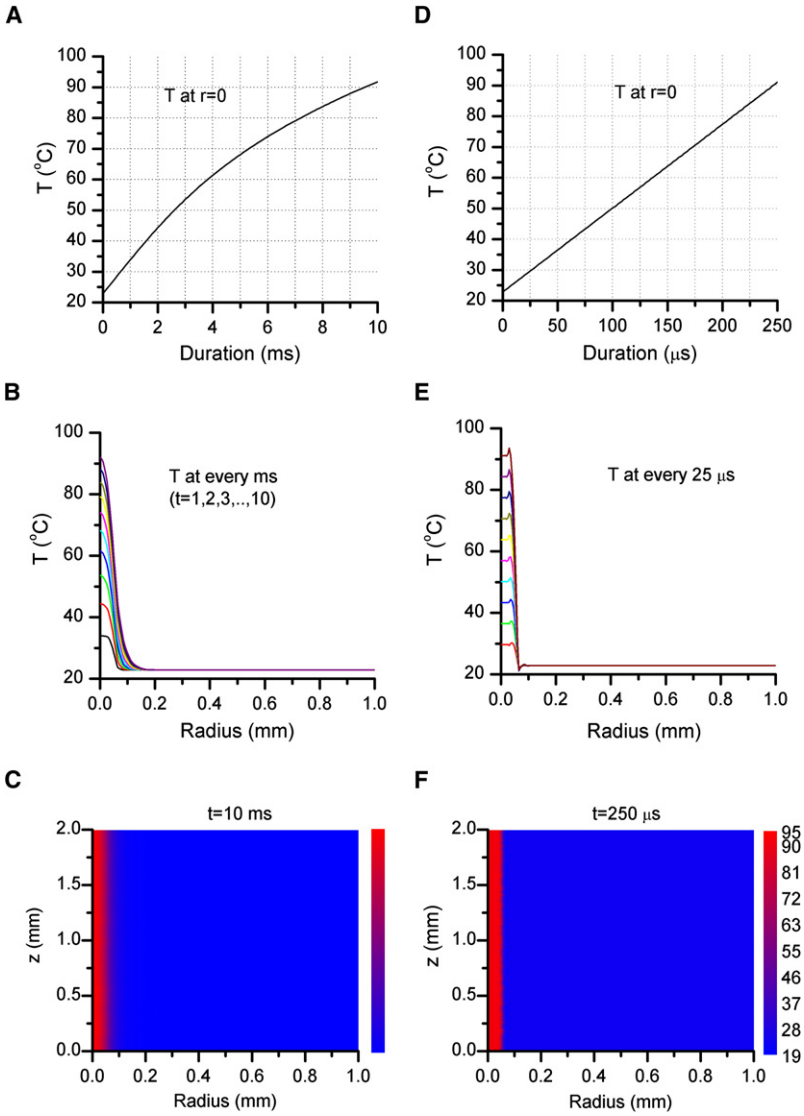

FIGURE 2 Simulation of laser-induced temperature changes. The left column corresponds to a laser beam of 8 W at 980 nm, whereas the right corresponds to a beam of 3 W at 1460 nm. (*A*) The time course of temperature at the beam center ($r = 0$, 980 nm). The increase of temperature was sublinear, as expected from diffusion of temperature away from the beam and heat loss occurring at a slower rate than light absorption. The rise time was ~4 ms for temperature from 22°C to 50°C (i.e., 10°C/ms). (*B*) Spatial profiles of temperature at different time as labeled. Temperature gradients were more significant at high temperatures. (*C*) Temperature distribution along the radial and optic axis. (*D–F*) Parallel plots for a laser beam of 3 W at 1460 nm. The temperature was nearly linear for temperature below ~90°C with a rate of ~280°C/ms. The spatial profile also exhibited a relatively uniform distribution within the beam ($r < 50$ μm). Simulation was carried out using COSMOL assuming a collimated beam of 100 μm diameter and standard values for water absorption coefficients ($\varepsilon = 30$ cm^{-1} at 1460 nm and 0.46 cm^{-1} at 980 nm) and heat capacity ($c_p = 4.2$ J/cm^3 × K). Starting temperature was 22°C. Laser powers were taken among the highest currently available for single-emitter diodes.

effectively clamped the temperature to its set point. The complete sequence of laser control pulses was recorded, along with the electrode current to a computer file. The first pulse duration for the initial heating determined the time responsiveness of the jump and was estimated from the target temperature. In practice, a sweep of temperature jumps spanning the entire responsive range of a channel were generated by varying the laser output power while maintaining the same initial heating duration (rise time).

Fig. 4 *B* illustrates an experimental recording of a constant temperature jump. The initial heating duration was set to 0.75 ms, producing a temperature rise from 23°C to 59°C, equivalent to ~50°C/ms. Modulation of the laser kept the electrode current, and thus the temperature, approximately constant. The fluctuation of temperature within the jump had a standard deviation $\sigma = 0.8$°C at 59°C ($\sigma/T = \sim 1\%$). The inset in Fig. 4 *B* shows an expanded view of the rising phase of the temperature jump. The rise of temperature was smooth without overshoot or ringing.

Because the laser control protocol synthesized with an open pipette was intended for use in subsequent experiments, we examined its repeatability. Fig. 4 *C* shows the current recorded with a newly installed electrode and stimulated with the laser control pulses previously generated. Alignment of the new electrode was aided using a video camera as described in Materials and Methods. As is evident from the figure, the current with the new electrode remained constant after the initial jump, and the rising phase was also similar. Fig. 4 *D* further plots the test temperature against the temperature in design. The two were tightly correlated over a broad range ($\delta_T/T \leq 0.5\%$, $n = 11$). These results indicate that constant temperature jumps were readily reproducible using this approach.

Patch-clamp studies

We examined the applicability and performance of laser-induced temperature jumps for patch-clamp experiments

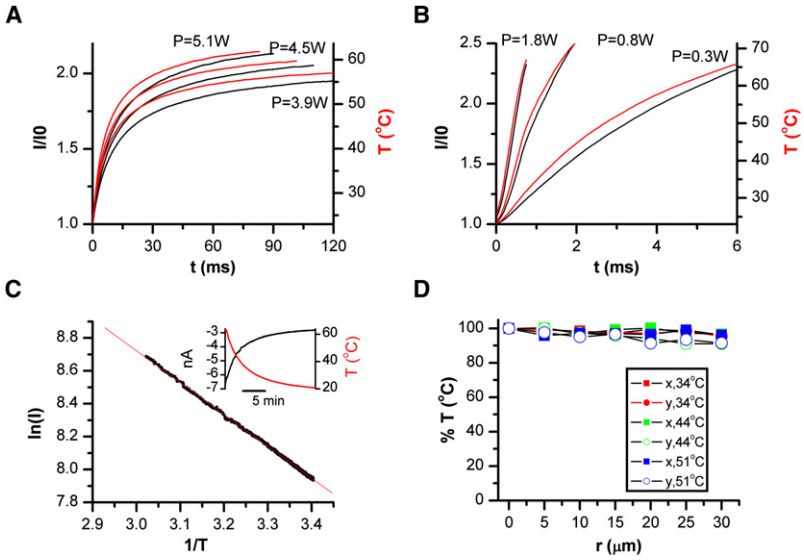

FIGURE 3 Experimental calibration. Temperature at the beam center was monitored by conductance changes of an open pipette. (*A* and *B*) Temperature after irradiation at (*A*) 980 nm or (*B*) 1460 nm. Different traces in each plot corresponding to different output powers. Pipette current is shown in black, whereas the calibrated temperature is in red/grey. The pipette was held at 30 mV. For a given current I, the temperature was calculated by $T = [1/T_0 - R/E_a \times \ln(I/I_0)]^{-1}$ where R is the gas constant, E_a the activation energy of electrolyte, and T_0 and I_0 are respectively the base (room) temperature and the corresponding electrode current. (*C*) Arrhenius plot of electrode current. For measurement, the chamber solution was preheated to ~60°C and then passively cooled while the temperature of the solution was recorded simultaneously with the pipette current using a thermistor immersed in the chamber (*inset* shows an example of recordings). The Arrhenius plot was linear over the tested temperatures (23°C to 60°C). The slope of the plot gave an average $E_a = 3.84 \pm 0.09$ kcal/mol ($n = 20$) for the control bath solution. (*D*) Spatial variation of temperature within the beam at 1460 nm. The tip of an open pipette was moved radially away from the beam center while the temperature at each spot was measured. The average deviation was <5% at $r \leq \pm 10$ μm, a radius larger than a typical HEK293 cell.

under various configurations, including macropatch, whole-cell and single-channel recording. For excised patch experiments, after excision the chamber was moved to a region free of cells and the patch was placed at the center of the laser beam. Fig. 5 shows a family of macroscopic currents recorded from an outside-out patch pulled from a HEK293 cell expressing TRPV1. Multiple temperature pulses from 36°C to 56°C with a duration of 100 ms and rise time of 0.75 ms were applied. At −100 mV, temperature-induced current began at >41°C, consistent with the threshold measured by resistive or thermal electric heating. As temperature increased, both the steady-state current and the activation rate increased rapidly and appeared to saturate at ~53°C. Subsequent heating to 56°C produced no further changes. The time course of the activation followed a single exponential at each temperature. At 53°C, the time constant was

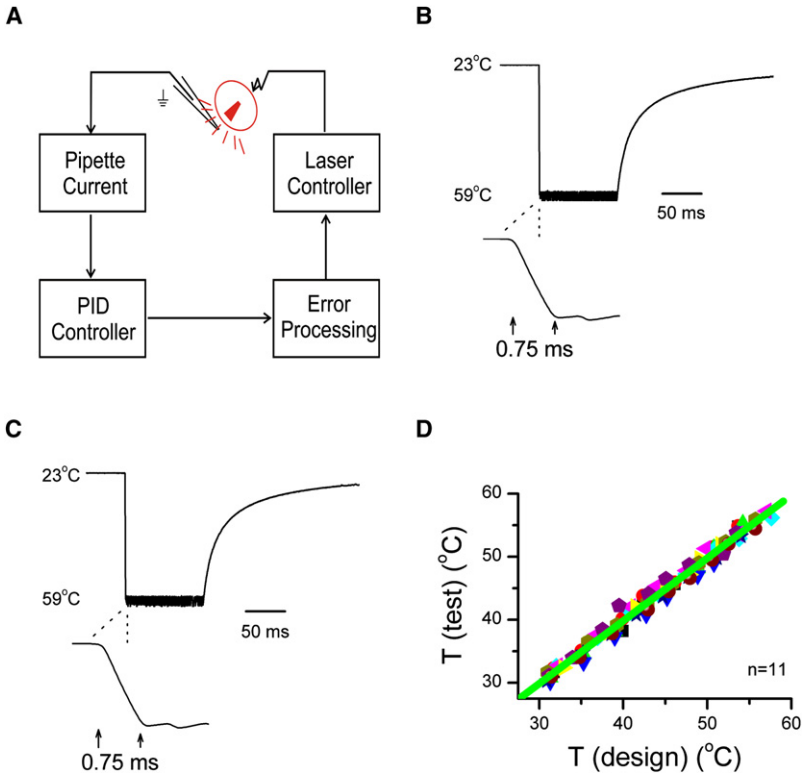

FIGURE 4 Implementation of constant temperature jumps. (*A*) A diagram of the feedback control. The diode current was modulated so that the current of an open pipette approximated a step response. The diode was initially pulsed on for a brief duration to reach the set point and was subsequently switched on and off to hold the electrode current to be constant. (*B*) An example of a constant temperature jump (shown as recorded current filtered at 2 kHz) from 23°C to 59°C in ~0.75 ms and maintained constant for 100 ms. Shown below is an expanded view of the rising phase. Within, the pulse temperature had a standard deviation $\sigma = 0.8$°C at 59°C (σ/T = ~1%). (*C*) Repeatability of constant temperature jumps. The temperature jump was recorded using a new electrode and stimulated with prerecorded pulse protocol. (*D*) Correlation plot of test temperatures against temperatures in the initial design, showing reproducibility over a broad range ($\delta_T/T \leq 0.5\%$, $n = 11$).

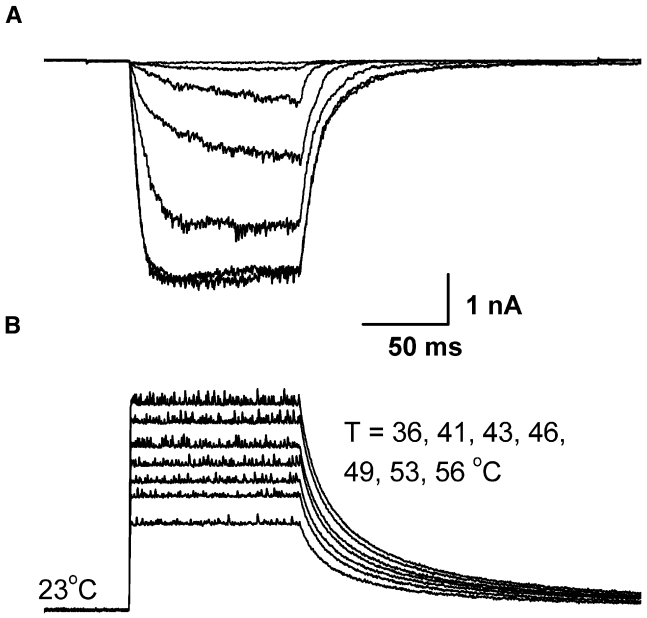

FIGURE 5 Application to macropatch recording. (*Bottom*) Temperature steps from 36°C to 56°C with a pulse duration of 100 ms and rise time of 0.75 ms (1460 nm). (*Top*) Current recordings from an outside-out macropatch excised from a HEK293 cell expressing TRPV1. Holding potential $V_h = -100$ mV. Significant currents occurred at ~41°C and increased rapidly with temperature. The activation time course in response to each temperature jump could be fitted to a single exponential (not shown). The activation reached saturation at ~53°C and had a time constant ~5 ms.

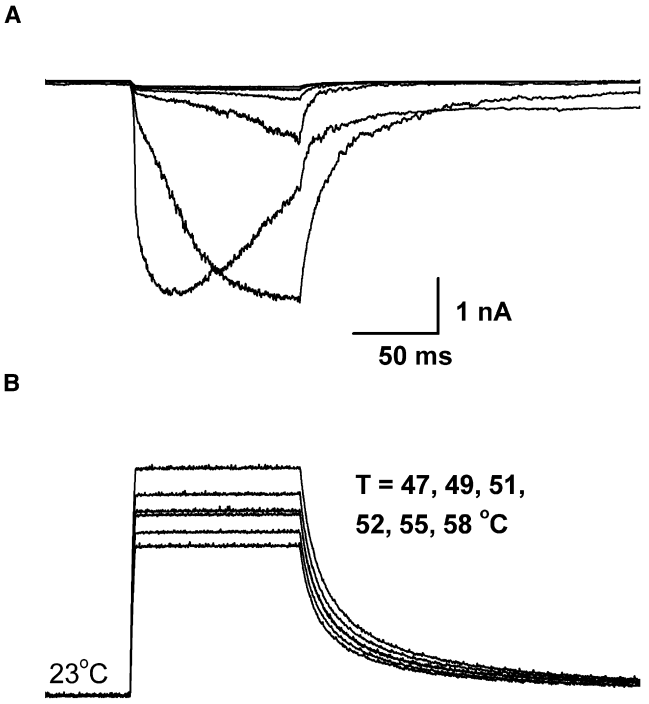

FIGURE 6 Activation of TRPV2 by temperature jumps. (*Bottom*) Temperature pulses ranging from 47°C to 58°C. The pulse duration was 100 ms, and the rise time was ~3 ms. (*Top*) Currents from an outside-out macropatch from a HEK 293 cell transiently transfected with TRPV2. Holding potential $V_h = -60$ mV. Significant currents were activated at temperature $\geq$52°C, and large increases occurred over a temperature change of ~4°C (from 51°C to 55°C). At the extreme temperature (~58°C), the current became inactivating, with a peak response similar to the steady-state current at 55°C. The rising phase time constant was ~34 ms at 55°C.

~5 ms, which was in the range of the open and closed dwell-time durations (11). This time constant was considerably slower than the rise time of temperature jumps (0.75 ms), supporting the feasibility of our approach for time-resolved measurements.

Fig. 6 shows a macropatch recording for another heat-activated ion channel, TRPV2. A small, slowly activating current began at ~51°C. This threshold agrees with a previous report that the channel is physiologically involved in detection of noxious heat above 50°C (3). Increasing the temperature to 55°C resulted in a large, slowly activating response. The current during the temperature step did not inactivate, but further increasing the temperature to 58°C led to a transient response. The activation rate was considerably faster than at 55°C, but the peak current was similar. This apparent inactivation was observed in several patches that sustained the high temperature, suggesting that it is either due to intrinsic inactivation of the channel or loss of functional channels. Exponential fitting of the response at 55°C gave a time constant ~34 ms, considerably slower than TRPV1.

Fig. 7 illustrates the application to whole-cell recording of an HEK293 cell transfected with TRPV1. Before patching, the cell was moved to the center of laser beam. The test temperatures were similar to those used in the macropatch recording, consisting of a family of constant temperature jumps from 39°C to 55°C with a pulse duration of 100 ms and rise time of 0.75 ms. Again, significant activation started at ~42°C and as temperature increased, the kinetics and the steady-state current increased. The time course of the response was exponential, with a time constant of 4.7 ms at 53°C. At steady state, the current was approximately constant, confirming that the temperature jump was stable. Control cells that were not transfected exhibited little activity in response to temperature jumps up to 50°C (data not shown).

Last, we examined the use of the system for single-channel experiments. Fig. 8 provides exemplar traces of single-channel recordings from an outside-out patch excised from a TRPV3-expressing oocyte. The patch was exposed to constant temperatures of 35°C, 40°C, and 44°C. Here, instead of varying laser diode power, we varied the duration of the initial pulse. As expected, the elevated temperature led to increases in open probability. The opening was sporadic at 35°C, but at 44°C, two channels appeared. The first latency of opening decreased considerably at 40°C, suggesting that the channel could be rapidly activated. The amplitude of the unitary current increased with temperature ($i = 14$, 16, and 18 pA at 35°C, 40°C, and 44°C respectively), and stayed relatively unchanged during each temperature pulse indicating that the temperature jump was clamped. At a

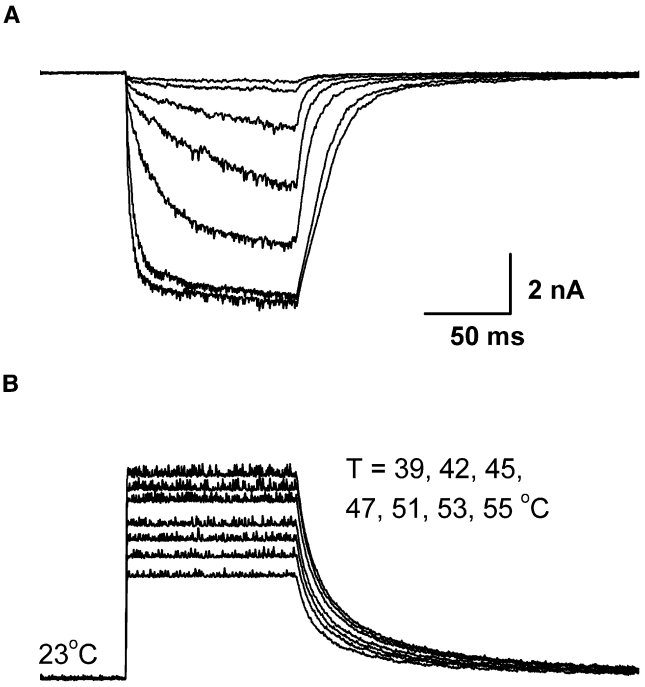

FIGURE 7 Application to whole-cell recording. (*Top*) Whole-cell currents from a HEK 293 cell transiently expressing TRPV1 (holding potential −60 mV), evoked by temperature steps from 39°C to 55°C. (*Bottom*) 100 ms pulse duration and 0.75 ms rise time. The channel started to be activated at 42°C and appeared to saturate at 53°C. In between, small changes of temperature resulted in large increases in currents. At 53°C, the activation had a time constant ~4.7 ms.

bandwidth of 2 kHz, the signal/noise ratio was >13. Thus, the fluctuation resulting from laser pulse modulation was small relative to the current amplitude of the channel, further supporting the applicability of the approach for single-channel measurements.

DISCUSSION

We have described a cost-effective approach for rapid temperature jumps for electrophysiological studies. The approach used high power infrared diode laser as a heat source. Laser beam from the diode was coupled to a fiber to restrict the irradiation area, thereby maximizing the rate of local temperature change. With an optical power <2 W at 1460 nm, we generated temperature jumps to ≥60°C with submillisecond rise times. Temperature ramps could be produced by irradiation at a constant power. Constant temperature jumps were implemented by pulse modulation of diode output using the conductivity of an open pipette as a feedback control signal. Patch-clamp experiments demonstrated the applicability of the approach for rapid local temperature perturbation of live cells and patches.

Effects of laser irradiation have been tested on cultured ganglion neurons. Small thermal effects were detected in earlier attempts due to the low power (<200 mW) (25,26). With a diode laser of 0.5W at 970 nm, Baumann and Martenson (24) were able to evoke trains of action potentials in cultured trigeminal neurons in response to stimuli of 45°C. More recently, Greffrath et al. (27) used a similar wavelength but much more powerful laser (10W at 980 nm) and showed possible activation of inward currents by laser irradiation in dissociated DRG neurons. The current had a nonlinear temperature dependence similar to temperature-evoked currents in nociceptive neurons elicited by superfusion of hot solutions (29–32). The time course of the current was slow, with an onset latency of ~300 ms. This slow time course appeared to result from the limited rise time of the stimuli (~30°C/400 ms). The current also increased without saturation due to continuous irradiation without feedback.

Our simulations showed that the 980 nm laser diode at 8 W had a response time on the order of ~5 ms for a temperature jump to >50°C (saturating temperature of heat-gated ion channels). This resolution is on the same order as channel kinetics (~5 ms for TRPV1). Thus, the 980 nm diode is inadequate for time-resolved detection of TRPV1. The 1460 nm laser is more efficient because water has a much higher extinction coefficient at 1460 nm (30 cm^{-1} vs. 0.46 cm^{-1} at 980 nm). The laser beam at 1460 nm is thus effectively ~65-fold more powerful than the 980 nm beam at equal power. Although single-emitter laser diodes at 980 nm have a power ~3–4-fold as high as at 1460 nm, the difference is insufficient to offset that in the absorption efficiency. Laser irradiation may cause cell or molecular damage but in this study we observed no evidence of such problems. Testing with several heat-gated channels showed a temperature dependence similar to that obtained by thermoelectric heating. Furthermore, the activation was repeatable even at extreme temperatures, suggesting that laser irradiation did not compromise function.

Using the resistance of a pipette as an indicator of local temperature is well established (27,29,33). The approach appeared accurate because the Arrhenius plot of the electrode current was linear over a large temperature range. The lookup table approach of predesigning laser control protocols with an open pipette was robust and efficient and had a maximum temporal responsiveness. Repeatability was reliable under a microscope with a video camera. One possible solution for real-time detection of temperature gradients would be to use temperature-sensitive fluorescent dyes, but we found that they had problems of either low temperature sensitivity or rapid bleaching, which complicated the calibration of temperature. The feasibility of the approach, especially its applicability to excised patches, needs to be investigated further.

Two important parameters for a constant temperature step are the rise time and the ripple size of fluctuations around the set point. The laser power, not the driving electronics, is likely to be a limiting factor for the time responsiveness. Diodes with a wavelength ~1500 nm are currently limited to an optical power in the range of a few watts. The simulations predicted that the rise time in this available power range

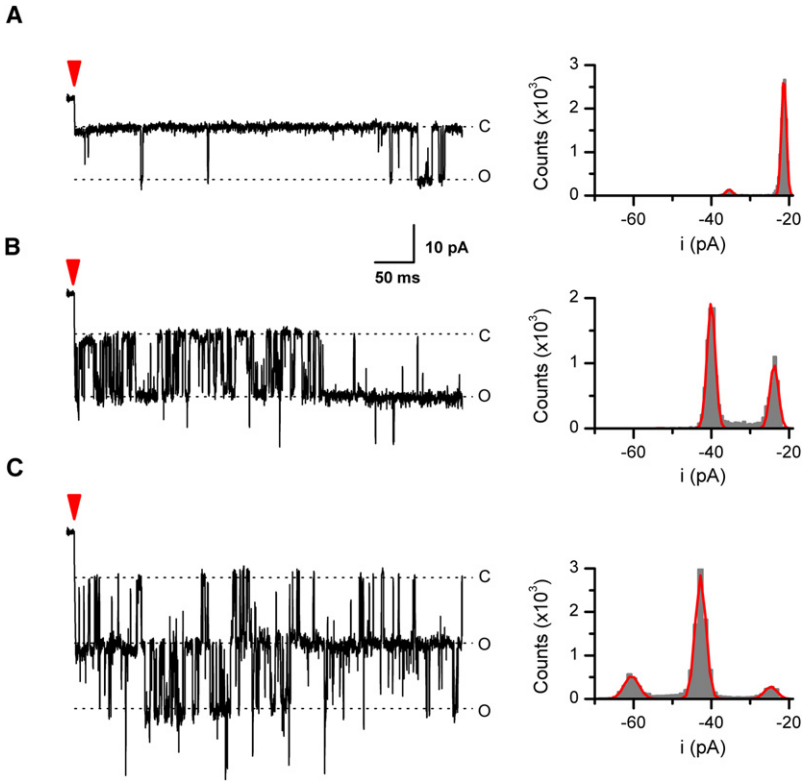

FIGURE 8 Application to single-channel recording. Activity of mTRPV3 in an outside-out patch at 35°C, 40°C, and 44°C was shown. The temperature pulse was 500 ms with a rise time of 1–2 ms. The arrow indicates the start of each pulse. The patch was excised from a *Xenopus* oocyte expressing mTRPV3. Holding potential −60 mV and data low-pass filtered at 2 kHz. Shown on the right are amplitude histograms along with their Gaussian fits (i = ~14, 16, and 18 pA at 35°C, 40°C, and 44°C, respectively).

is limited to a few hundred microseconds. The steady-state noise from pulse modulation depends on the feedback control algorithm. In our current implementation, we used a quasi-CW current source that can operate in both pulsing and continuous mode and therefore allows for a simple on-and-off modulation to maintain constant temperature. It is relatively straightforward to implement but introduced coupling between the laser power and the ripple size of fluctuations. Further improvement to full proportional-integral-derivative control could minimize the fluctuations if necessary.

Our patch-clamp experiments showed that thermal TRP ion channels can be activated rapidly by temperature. The activation of TRPV1 had a time constant on the order of 5 ms at −100 mV, comparable to ligand- or voltage-gated ion channels. The gating of a temperature-activated ion channel necessitates large enthalpy and entropy changes (11–13,30). Our previous single-channel analysis on heat activation of TRPV1 estimated a temperature dependence of $Q_{10} \approx 7$ for the duration of long closures between opening bursts, which reflected the opening rate (11). This value of Q_{10} corresponds to an activation enthalpy 2–3-fold as large as that for ligand- or voltage-gated ion channels ($Q_{10} = 2$–3). Apparently, the temperature gating in these channels was able to traverse the large energy barrier as rapidly as the gating by voltage or ligand binding. The rapid activation kinetics suggest that the energetic sources for the high temperature dependence are likely localized and close to the channel. The ability to perform fast temperature jumps will enable further nonequilibrium measurements on these thermal TRPs, which will be important for interrogating the mechanisms of thermosensitivity.

We thank Dr. Fred Sachs for critical reading of the manuscript.

This work was supported by grant R01-GM65994 from National Institutes of Health.

REFERENCES

1. Hille, B. 2001. Ion Channels of Excitable Membranes. Sinauer Associates, Sunderland, Massachusetts.
2. Caterina, M. J., M. A. Schumacher, M. Tominaga, T. A. Rosen, J. D. Levine, et al. 1997. The capsaicin receptor: a heat-activated ion channel in the pain pathway. *Nature*. 389:816–824.
3. Caterina, M. J., T. A. Rosen, M. Tominaga, A. J. Brake, and D. Julius. 1999. A capsaicin-receptor homologue with a high threshold for noxious heat. *Nature*. 398:436–441.
4. Peier, A. M., A. J. Reeve, D. A. Andersson, A. Moqrich, T. J. Earley, et al. 2002. A heat-sensitive TRP channel expressed in keratinocytes. *Science*. 296:2046–2049.
5. Xu, H. X., I. S. Ramsey, S. A. Kotecha, M. M. Moran, J. H. A. Chong, et al. 2002. TRPV3 is a calcium-permeable temperature-sensitive cation channel. *Nature*. 418:181–186.
6. Smith, G. D., J. Gunthorpe, R. E. Kelsell, P. D. Hayes, P. Reilly, et al. 2002. TRPV3 is a temperature-sensitive vanilloid receptor-like protein. *Nature*. 418:186–190.
7. Guler, A. D., H. Lee, T. Iida, I. Shimizu, M. Tominaga, et al. 2002. Heat-evoked activation of the ion channel, TRPV4. *J. Neurosci.* 22:6408–6414.
8. McKemy, D. D., W. M. Neuhausser, and D. Julius. 2002. Identification of a cold receptor reveals a general role for TRP channels in thermosensation. *Nature*. 416:52–58.

9. Peier, A. M., A. Moqrich, A. C. Hergarden, A. J. Reeve, D. A. Andersson, et al. 2002. A TRP Channel that Senses Cold Stimuli and Menthol. *Cell*. 108:705–715.
10. Story, G. M., A. M. Peier, A. J. Reeve, S. R. Eid, J. Mosbacher, et al. 2003. ANKTM1, a TRP-like channel expressed in nociceptive neurons, is activated by cold temperatures. *Cell*. 112:819–829.
11. Liu, B., K. Hui, and F. Qin. 2003. Thermodynamics of heat activation of single capsaicin ion channels VR1. *Biophys. J.* 85:2988–3006.
12. Brauchi, S., P. Orio, and R. Latorre. 2004. Clues to understanding cold sensation: thermodynamics and electrophysiological analysis of the cold receptor TRPM8. *Proc. Natl. Acad. Sci. USA*. 101:15494–15499.
13. Voets, T., G. Droogmans, U. Wissenbach, A. Janssens, V. Flockerzi, et al. 2004. The principle of temperature-dependent gating in cold- and heat-sensitive TRP channels. *Nature*. 430:748–754.
14. Grandl, J., H. Hu, M. Bandell, B. Bursulaya, M. Schmidt, et al. 2008. Pore region of TRPV3 ion channel is specifically required for heat activation. *Nat. Neurosci.* 11:1007–1013.
15. Pennell, T., T. Suchyna, J. Wang, J. Heo, J. D. Felske, et al. 2008. Microfluidic chip to produce temperature jumps for electrophysiology. *Anal. Chem.* 80:2447–2451.
16. Moore, L. E., J. P. Holt, Jr., and B. D. Lindley. 1972. Laser temperature-jump technique for relaxation studies of the ionic conductances in myelinated nerve fibers. *Biophys. J.* 12:157–174.
17. Thompson, P. A., W. A. Eaton, and J. Hofrichter. 1997. Laser temperature jump study of the helix<==>coil kinetics of an alanine peptide interpreted with a 'kinetic zipper' model. *Biochemistry*. 36:9200–9210.
18. Williams, S., T. P. Causgrove, R. Gilmanshin, K. S. Fang, R. H. Callender, et al. 1996. Fast events in protein folding: helix melting and formation in a small peptide. *Biochemistry*. 35:691–697.
19. Petty, S. A., and M. Volk. 2004. Fast folding dynamics of an α-helical peptide with bulky side chains. *Phys. Chem. Chem. Phys.* 6:1022–1030.
20. Phillips, C. M., Y. Mizutani, and R. M. Hochstrasser. 1995. Ultrafast thermally induced unfolding of RNase A. *Proc. Natl. Acad. Sci. USA*. 92:7292–7296.
21. Spiegel, J., C. Hansen, and R. D. Treede. 2000. Clinical evaluation criteria for the assessment of impaired pain sensitivity by thulium-laser evoked potentials. *Clin. Neurophysiol.* 111:725–735.
22. Wells, J., C. Kao, P. Konrad, T. Milner, J. Kim, et al. 2007. Biophysical mechanisms of transient optical stimulation of peripheral nerve. *Biophys. J.* 93:2567–2580.
23. Veldhuijzen, D. S., M. I. Nemenov, M. Keaser, J. Zhuo, R. P. Gullapalli, et al. 2009. Differential brain activation associated with laser-evoked burning and pricking pain: an event-related fMRI study. *Pain*. 141:104–113.
24. Baumann, T. K., and M. E. Martenson. 1994. Thermosensitivity of cultured trigeminal neurons. *Abstr. Soc. Neurosci.* 20:1379.
25. Miura, A., and M. Kawatani. 1996. Effects of diode laser irradiation on sensory ganglion cells from the rat. *Pain Res.* 11:175–183.
26. Jimbo, K., K. Noda, K. Suzuki, and K. Yoda. 1998. Suppressive effects of low-power laser irradiation on bradykinin evoked action potentials in cultured murine dorsal root ganglion cells. *Neurosci. Lett.* 240:93–96.
27. Greffrath, W., M. I. Nemenov, S. Schwarz, U. Baumgartner, H. Vogel, L. Arendt-Nielsen, and R. D. Treede. 2002. Inward currents in primary nociceptive neurons of the rat and pain sensations in humans elicited by infrared diode laser pulses. *Pain*. 99:145–155.
28. Hui, K. Y., B. Y. Liu, and F. Qin. 2003. Capsaicin activation of the pain receptor, VR1: multiple open states from both partial and full binding. *Biophys. J.* 84:2957–2968.
29. Cesare, P., and P. McNaughton. 1996. A novel heat-activated current in nociceptive neurons and its sensitization by bradykinin. *Proc. Natl. Acad. Sci. USA*. 93:15435–15439.
30. Vyklicky, L., V. Vlachova, Z. Vitaskova, I. Dittert, M. Kabat, et al. 1999. Temperature coefficient of membrane currents induced by noxious heat in sensory neurones in the rat. *J. Physiol.* 517:181–192.
31. Nagy, I., and H. Rang. 1999. Noxious heat activates all capsaicin-sensitive and also a sub-population of capsaicin-insensitive dorsal root ganglion neurons. *Neuroscience*. 88:995–997.
32. Liu, L., and S. A. Simon. 2000. Capsaicin, acid and heat-evoked currents in rat trigeminal ganglion neurons: relationship to functional VR1 receptors. *Physiol. Behav.* 69:363–378.
33. Auerbach, A., F. Sachs, J. Neil, and R. McGarrigle. 1986. Temperature measurement and control of small volumes: applications for single channel recording. *Methods Enzymol.* 124:190–206.